energies

MDPI

Article

Effects of Porous Structure Development and Ash on the Steam Gasification Reactivity of Biochar Residues from a Commercial Gasifier at Different Temperatures

Saiman Ding, Efthymios Kantarelis and Klas Engvall *

Department of Chemical Engineering, KTH Royal Institute of Technology, SE-100 44 Stockholm, Sweden; saiman@kth.se (S.D.); ekan@kth.se (E.K.)

* Correspondence: kengvall@kth.se

Received: 18 August 2020; Accepted: 19 September 2020; Published: 23 September 2020

Abstract: The present study aims at investigating the effects of porous structure development and ash content on the observed reactivity during steam gasification of biochar residues from a commercial gasifier. The experiments were conducted at a temperature range of 700 to 800 °C using biochar, derived from entrained flow gasification of biomass, under isothermal conditions using a thermogravimetric analyzer. The pore size distribution, surface area and morphology of char samples were determined by N_2 physiosorption and scanning electron microscopy (SEM). The results showed that the gasification temperature does not affect the porous structure development considerably. The total surface area of char exhibits a threefold increase, while the total pore volume increase ranges between 2.0 and 5.3 times, at all temperatures. Both properties are directly proportional to the observed reactivity, especially at conversions up to 70%. Catalytic effects of the mineral matter of the char (mainly potassium) become predominant at the later stages of conversion (conversion greater than 70%).

Keywords: steam gasification; char reactivity; pore structure; ash effects

1. Introduction

With the increasing energy demand and the environmental impact by the use of fossil fuel, biomass waste feedstocks, such as forestry residue and agricultural waste, are becoming an attractive resource for renewable energy [1]. A feasible technique for primary conversion of biomass waste feedstocks into an intermediate gaseous feedstock (suitable for further upgrading to useful end user products, such as chemicals, heat, and power) is gasification [2]. The biomass conversion includes several consecutive steps, such as drying, pyrolysis, gasification, or partial combustion of the residual char, as well as homogeneous gas phase reactions. The gasification of char, produced in the pyrolysis step, consists of a set of heterogeneous reactions with gasifying agents, such as CO_2, H_2O, and O_2, and is generally the rate-determining step [3]. An understanding of the mechanism and kinetics of char gasification is important to provide useful data for gasification reactor design.

Reports on gasification and combustion reactivity and kinetics of coal and coal char are extensive [4–7], as compared to a more limited number of studies on lignocellulosic char (or biochar) reactivity. There are many similarities between the two feedstocks, but the biochar is far more reactive (4–10 times) as a result of their physicochemical properties [8]. Information on the reactivity and kinetics of lignocellulosic char can be found in the comprehensive review by Di Blasi [9].

Char gasification is generally influenced by a number of different parameters such as temperature, particle size, char pore structure, and intrinsic char reactivity [9]. Furthermore, the particle temperature history of char generation influence its reactivity [10]. For example, Septien et al. [11] reported that

increased pyrolysis heating rates (from 1 °C/s to 1000 °C/s) result in higher gasification rates and also to a more reactive solid char. The higher reaction rate (i.e., char reactivity) may be attributed to a change in morphology [12] or a change in textural properties due to the formation of a larger pore volume at high heating rates, mainly consisting of mesopores and macropores, compared to a lower pore volume of mainly micropores at a low heating rates [13]. Textural biomass-char properties are also significantly changed during the gasification process, expressed as an evident increase in porosity and surface area [14–22]. Most studies on pore structure development of biomass char use CO_2 as the gasification agent [14–17,22] and only a few studies focus on char steam gasification, especially wood-derived chars, at different temperatures [18,19,23].

Another important factor influencing the reactivity is the mineral content and composition in the char. Alkali and alkaline earth metals (AAEMs) such as potassium, sodium, calcium, and magnesium, act as catalysts and accelerate the char gasification process, favoring heterogeneous char-steam, char-O_2, and char-CO_2 reactions [24–33].

The majority of studies of biochar reactivity generally use biochar samples produced in a pyrolysis step at lab-scale either directly in thermobalances, including thermogravimetric analysis (TGA) instruments [29,34] and fixed bed reactors [33], in drop tubes [31,35] or fluidized beds [28,36]. Detailed studies on reactivity of char, collected at commercial or demonstration scale gasification processes, so-called semi-char, are rarely found in the literature and corresponds to a few cases of coal semi-chars [35,37–40] and one case investigating different biomass semi-chars, collected from circulating fluidized bed (CFB) gasifiers [41]. The main results from the coal semi-char investigations are somewhat contradictory to each other, with studies observing a lower [37,40] and higher [35] gasification reactivity of char collected from fluidized bed gasifiers, compared to corresponding pyrolyzed coal chars. An example where coal semi-char from Texaco entrained flow slurry gasifiers is investigated is reported by Gu et al. [38]. They concluded that the chemical reactivity of two collected coal semi-chars was much higher compared to corresponding pyrolyzed chars. In case of biomass gasification, Meng et al. [41] investigated semi-char of wood pellets, willow, and dried distiller's grains with solubles (DDGS) collected from the downcomer in a pilot scale steam-O_2 blown CFB gasifier. Although not explicitly investigating the char reactivity, the calculated activation energy range of collected CFB semi-chars was lower, compared to the corresponding pyrolyzed chars, suggesting a higher reactivity of the semi-chars.

It is evident that the reactivity of a char differs depending on the conditions present in a real-scale gasification plant and also between chars produced in the laboratory and real chars. Most studies investigating steam biomass char gasification relate the observed reactivity to char structure development [17,19,20,22] or ash content [9,21,42–46] individually and not in synergy. Mechanistic studies on how both parameters contribute to the char reactivity of real biomass semi-char, during its transformation under steam gasification conditions, are important to enable the development of kinetic models. The present study, aims at evaluating a residual biomass semi-char, collected at a demonstration scale entrained flow gasification process (4 $MW_{th\ biomass}$) for combined heat and power production and compare the char reactivity properties with char equivalents in the literature. The biomass char was gasified to different degrees of conversion with steam in a thermogravimetric analyzer (TGA), where each sample of partially gasified char was characterized in terms of textural and morphological characteristics, as well as of ash contents on the surface. In order to evaluate the combined effects of the structural development and ash components on char reactivity, during steam gasification, ash-leached char samples were prepared and compared with the original char.

2. Method

2.1. Raw Material and Sample Preparation

The material used in the present work was unreacted biomass char, collected at a demonstration scale entrained flow gasifier, using pine wood with a maximum particle diameter of 0.1 mm (see

Supplementary Materials). The unreacted char was collected from the scrubber sedimentation tank, placed downstream of the gasifier. Biomass is gasified at temperatures ranging between 900 and 1150 °C using air as gasification agent at an equivalence ratio of 0.28–0.32.

Prior to use, the char residue was dried in at 105 °C overnight. In order to remove any residual volatile matter, the samples were heated at 950 °C in N_2 atmosphere for 3h. The sample was ground to a particle size of 45–120 µm. The resultant char is designated as original char (OC). The results of ultimate and proximate analyses, and mineral content, determined according to the American Society for Testing and Materials (ASTM) methods and ISO 29541:2010, respectively, of both the original biomass fed to the gasifier and the OC are reported in Table 1.

Table 1. Ultimate and proximate analyses of biomass and original char.

Proximate Analysis (wt%)		
	Biomass	**Original Char**
Moisture	7.2	0.6
Volatile Matter (db) [b]	92.8	4.53
Ash (db) [a]	0.32	6.9
Fixed carbon (db) [b]	6.88	88.57
Ultimate Analysis (wt% db)		
C	50.9	90.6
H	6.2	0.2
N	<0.1	0.43
O [b]	42.6	1.87
Mineral Matter (mg/kg db)		
Na	111	755
K	340	5690
Mg	114	2660
Ca	562	11,200
Fe	45.5	720
Al	79	336
Mn	69.9	1540
P	37.8	677
Si	43.1	1450

db-dry basis. [a] Determined at 550 °C, [b] Determined by difference.

In order to evaluate the effects of ash on char reactivity during steam gasification, ash-leached char samples were also prepared. Deionized water was used as a leaching agent to avoid damaging the char structure and hence affecting the char reactivity. Leaching was performed at 40 °C with a liquid to solid ratio (*v/w*) of 80 [47] under continuous stirring for 2 and 48 h in order to achieve a different degree of demineralization. After leaching, the samples were washed and dried at 105 °C overnight. The leached samples were named as 2LC and 48LC referring to 2 and 48 h of treatment, respectively. Mineral matter of original and leached chars were analyzed by ICP-SFMS.

2.2. Steam Char Gasification TGA Experiments

Char steam gasification experiments were carried out in isothermal conditions, using a NETZCSH ST490 F3 thermogravimetric analyzer (TGA). In each gasification experiment, approximately 30 ± 2 mg of char powder was loaded in a 3.4 mL ceramic crucible. The sample was initially heated at a rate of 10 °C/min in N_2 atmosphere (300 mL/min) to the desired temperature (700, 750, and 800 °C) and maintained for 5 min for temperature stabilization. The gasification took place in a 7.6 mol-% steam atmosphere. The char conversion (X) and reactivity (dX/dt) were calculated according to the following,

$$X = \frac{m_0 - m_t}{m_0 - m_{ash}} \ [-] \quad (1)$$

$$\frac{dX}{dt} = -\frac{1}{m_0 - m_{ash}} \frac{dm_t}{dt}, \ \left[\text{min}^{-1}\right]$$

where m_0 represents the initial mass of the char at the onset of gasification, m_t is the instantaneous mass of the char at time t, and m_{ash} is the residual mass of ash.

In order to study the development of the porous structure of char, the gasification reaction was stopped at different conversions aiming at capturing all the reactivity turning points that were observed during complete conversion (at least three to four points).

2.3. Textural Analysis (N_2 Physisorption)

The specific surface area and pore size distribution were determined by N_2 physisorption (Micromeritics ASAP 2000) based on the Brunauer–Emmett–Teller (BET) method [48,49]. Each sample was degassed at 250 °C overnight prior to analysis. The pore size distribution was determined using Barrett–Joyner–Halenda (BJH) method, while the micropore volume was determined using the t-plot method.

2.4. SEM Analysis

Samples' surface morphology was investigated by means of scanning electron microscopy (SEM) using a Zeiss GeminiSEM 450 at 15kV. SEM was coupled with energy-dispersive X-ray spectroscopy (EDX). Determination of surface elements concentration was performed using a Si (Li) detector and the Oxford INCA Energy software. The analyses were done in low vacuum mode with carbon tape under the sample. Average mineral content on char sample surface was determined from SEM images with 1000× magnification.

3. Results

All the tests conducted in the present work are presented in Table 2. For OC, textural and morphological characteristics were determined at different conversions. To ensure the repeatability of the runs, the mass loss curves at 700–800 °C at different conversions were compared (see Supplementary Materials (Figures S-2 to S-4)). It was found that the experimental error does not exceed 2%.

Table 2. Summary of experiments and analyses.

	700˚C					750 ˚C						800 ˚C					
Conversions (%)	0	27	64	72	100	0	27	53	73	91	100	0	25	45	70	85	100
Sample / Tests	OC																
TGA		✓	✓	✓	✓		✓	✓	✓	✓	✓		✓	✓	✓	✓	✓
BET	✓	✓	✓	✓		✓	✓	✓	✓	✓		✓	✓	✓	✓	✓	
SEM/EDS	✓	✓	✓	✓		✓	✓	✓	✓	✓		✓	✓	✓	✓	✓	
Samples / Tests	2LC and 48LC																
TGA					✓						✓						✓
BET	✓					✓						✓					
SEM/EDS	✓					✓						✓					

The reactivity of the TGA-produced char (from original biomass) and the gasifier-derived char (OC) were determined at 900 °C and are shown in Figure 1. As seen, the temperature history of the particle has an effect on the reactivity of the derived char. The gasifier-derived char (OC) shows almost half of the reactivity of the TGA produced char and shows an increasing reactivity at the later stages of the conversion.

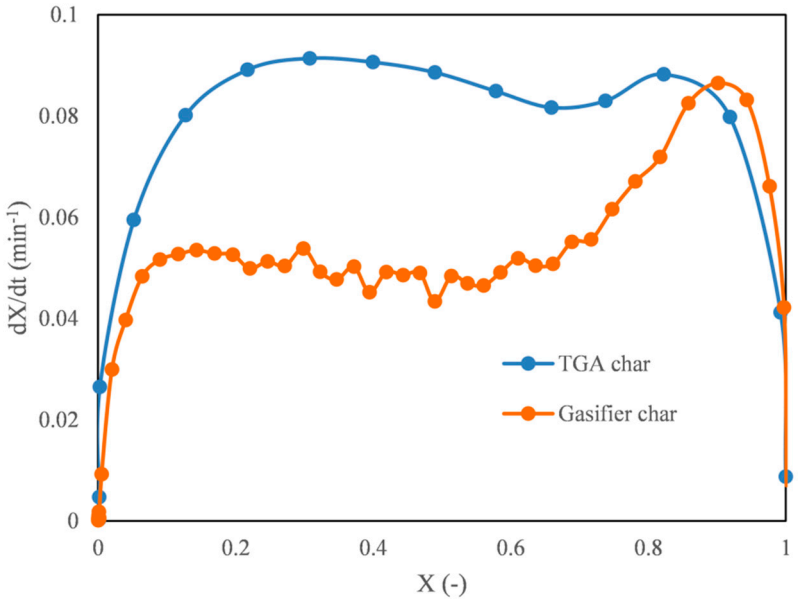

Figure 1. Reactivity of thermogravimetric analysis (TGA)-derived char as compared to the gasifier-derived char.

3.1. Original Char

The reactivity of char at 700, 750, and 800 °C is shown in Figures 2–4, respectively. As shown, there are two distinct regions of conversion where reactivity behavior is different; namely, conversion from 0 to 70% and from 70% to complete conversion. In the first region the reactivity is somewhat stable with decreasing trend while at conversions higher than 70%, the reactivity increases significantly.

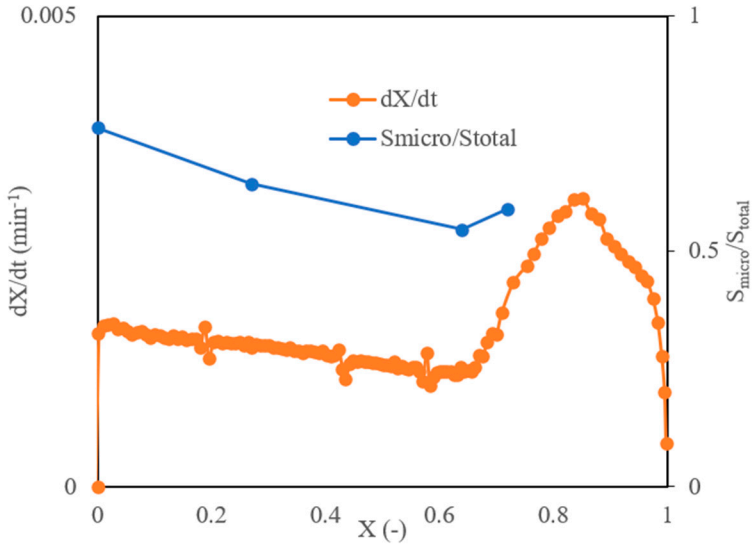

Figure 2. Micropores development and its reactivity at 700 °C.

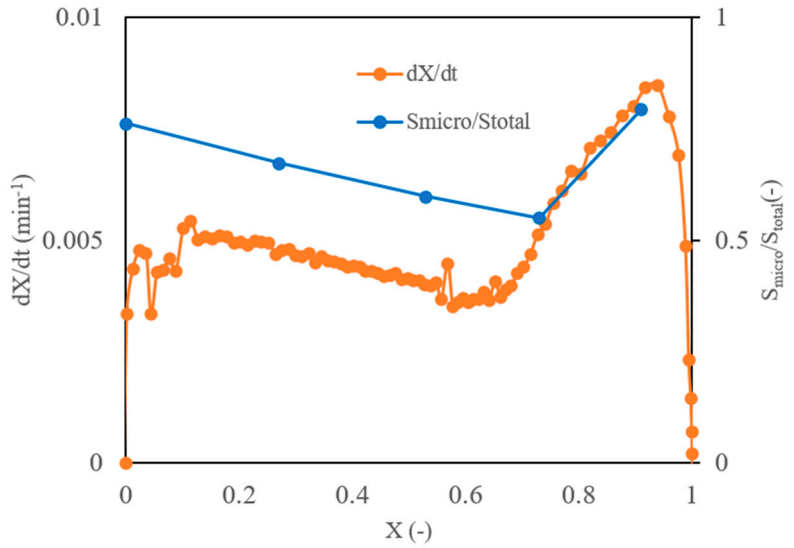

Figure 3. Micropores development and its reactivity at 750 °C.

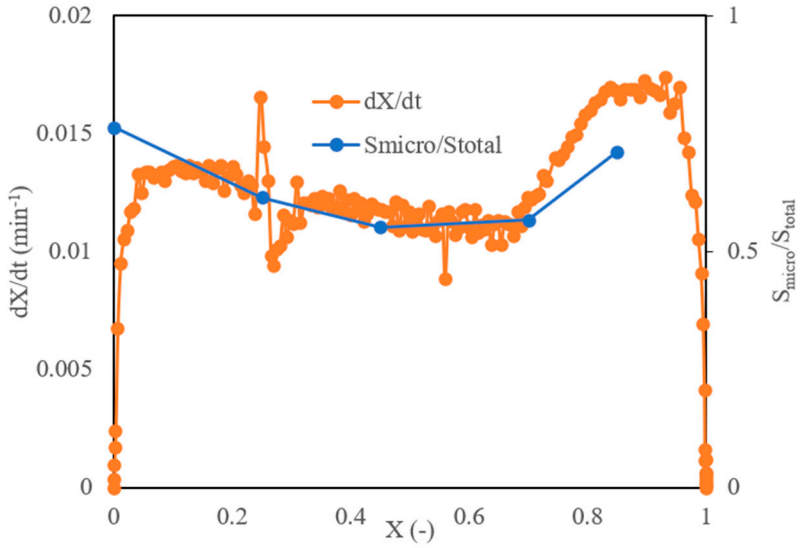

Figure 4. Micropores development and its reactivity at 800 °C.

Figure 5 illustrates the pore size distribution of the original char at different conversions and temperatures (700, 750, and 800 °C). As shown, at conversions higher than 70%, the mesopores (2–50 nm) fraction start to decrease at the expense of macropores showing a progressive pore growth. The pore volume in the macropore range (>50 nm) is positively correlated with the conversion.

The textural properties of the char at different temperatures and conversions for the original char can be seen in Figure 6. The multipoint BET method was used to calculate the specific surface area, with a relative error between 0.37% and 0.78%. As shown in Figure 6a,b the total pore volume (V_{total}) and the total specific surface area (S_{total}) increases 1.3–3.1 and 2.0–5.3 times, respectively, with conversion until a value of approximately 70% at all temperatures, indicating a formation of new pores, as a result of steam-carbon reaction. Similar results are also reported in other studies [17,22]. S_{total}, as well as V_{total}, start to decrease after this point. The fraction of micropores increases with conversion monotonically and constitute the majority of the surface area of the char. At 70%, a steep increase in V_{micro} and S_{micro} formation is observed. Figure 6b,d displays the increase of S_{total} and S_{micro} with conversion with a higher increase in the rate of S_{total} compared to S_{micro} until ~70% conversion. Therefore, the mesopores develop at a faster rate than micropores generated until this point. This result is inconsistent with Fu et al. [18], who observed an increase of the rate of S_{total} as S_{micro} kept

constant, when the conversion is higher than 10%. The discrepancy can be attributed to the different controlling regime as will be discussed later.

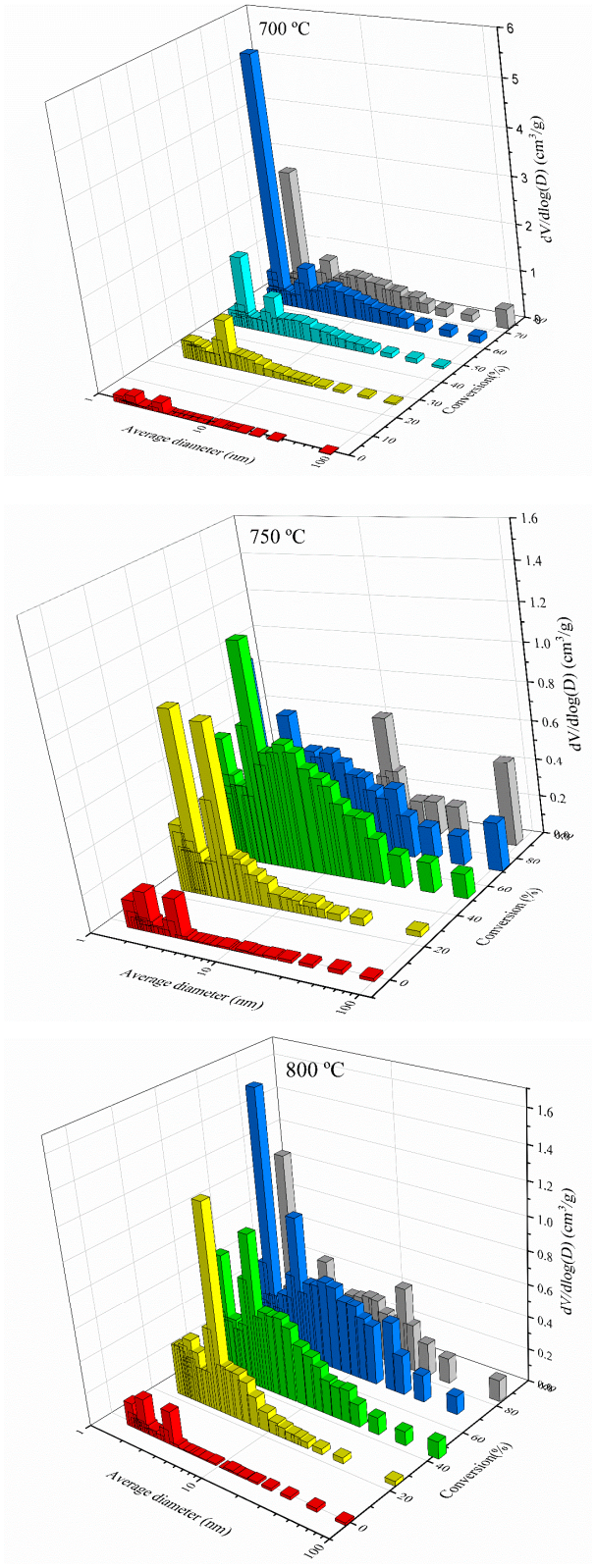

Figure 5. Pore size distribution of char at different conversions and 700, 750, and 800 °C according to Barrett–Joyner–Halenda (BJH) method.

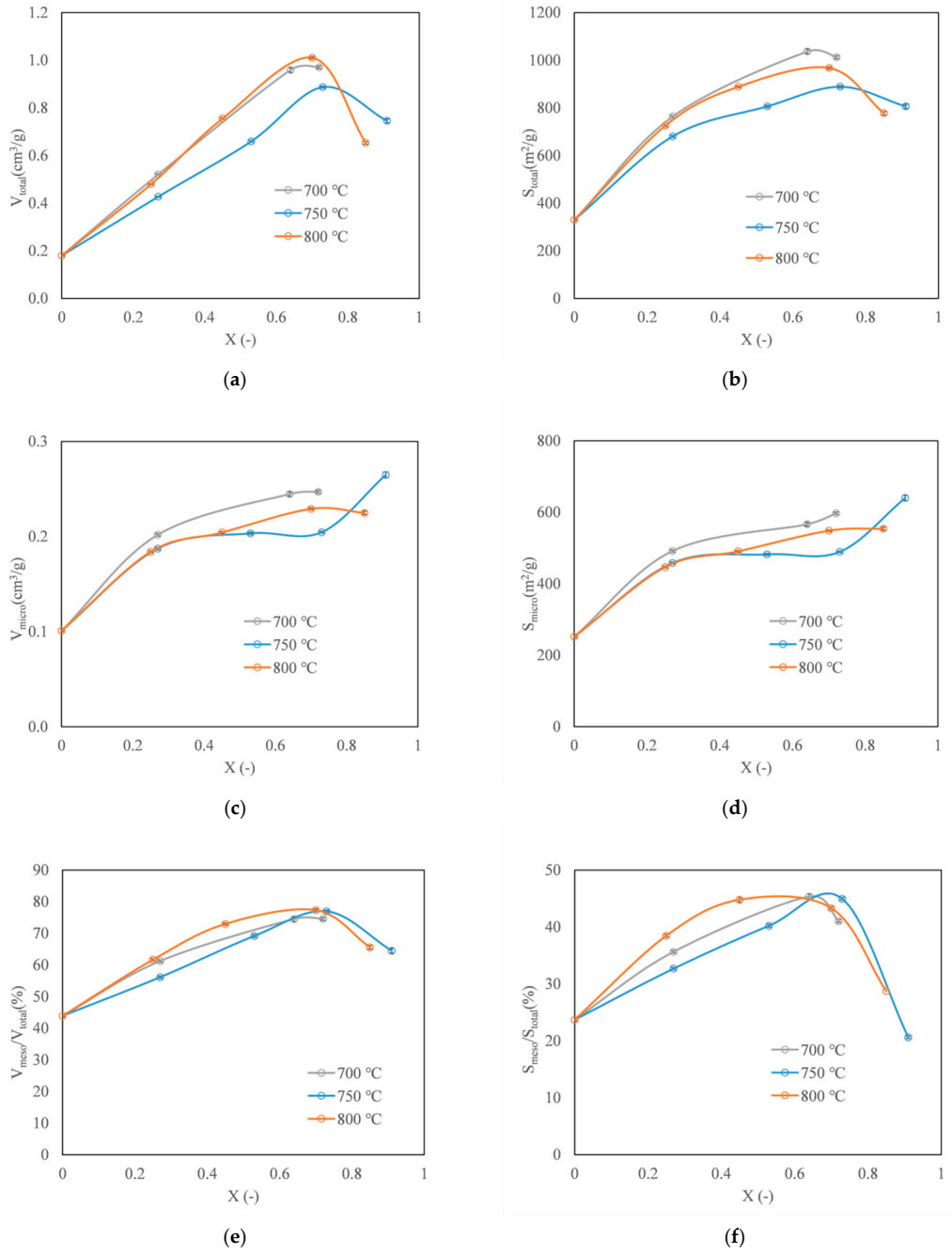

Figure 6. Textural properties of the OC at different temperatures with different conversions for original char. Left: pore volume versus conversion at different temperatures. Right: Specific surface area versus conversion at different temperatures. (The relative error is minor and is not shown in the figure.) (**a**) the total pore volume versus conversion; (**b**) the total specific surface area versus conversion; (**c**) the micropore volume versus conversion; (**d**) the micopore surface area versus conversion; (**e**) the mesopores volume fraction versus conversion; (**f**) the mesopore area fraction versus conversion.

As shown in Figure 6e,f, the mesopores volume fraction increases from 44% to 77% until 70% conversion, while the mesopore area fraction increases from 24% to 45%. At conversions higher than ~70%, the volume fraction of the mesopores decreases from 77% to ~65%. Similarly, the mesopores fraction in the total surface area decreases from 45% to 20%.

At different gasification temperatures, the S_{micro}/S_{total} ratio curve is almost identical to the changes in the reactivity (Figures 2–4). In the conversion range from 0 to 70%, the reactivity decreases and so

does the S_{micro}/S_{total} ratio. After 70% conversion, the reactivity and S_{micro}/S_{total} ratio starts to increase significantly. This behavior may be related to the generation of new micropores, resulting in an extended surface area for heterogeneous steam-carbon reaction, which leads to increased reactivity.

SEM images (with 1000× magnification) of original char and gasified chars at different carbon conversions, from gasification at 700, 750 and 800 °C in 30 mol-% steam atmosphere, are shown in Figures 7–10 (500× and 100× magnifications are presented in the Supplementary Materials (Figures S-5 to S-11). As shown, the surface of the original char is quite porous (as also confirmed by the BET measurements); sparse minerals particles, mainly Ca, is distributed thinly on the char surface (see Supplementary Material for additional information). During the gasification reaction, the carbon is continuously consumed, and pores of gasified chars are expanding and increasing.

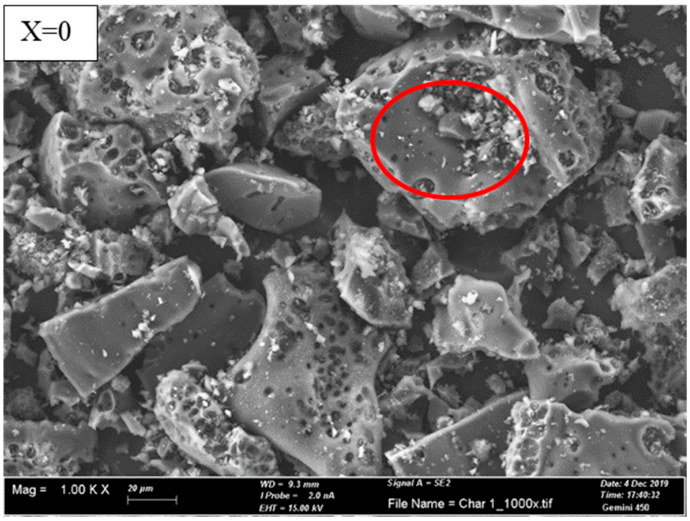

Figure 7. SEM images (1000× magnification) of the original char.

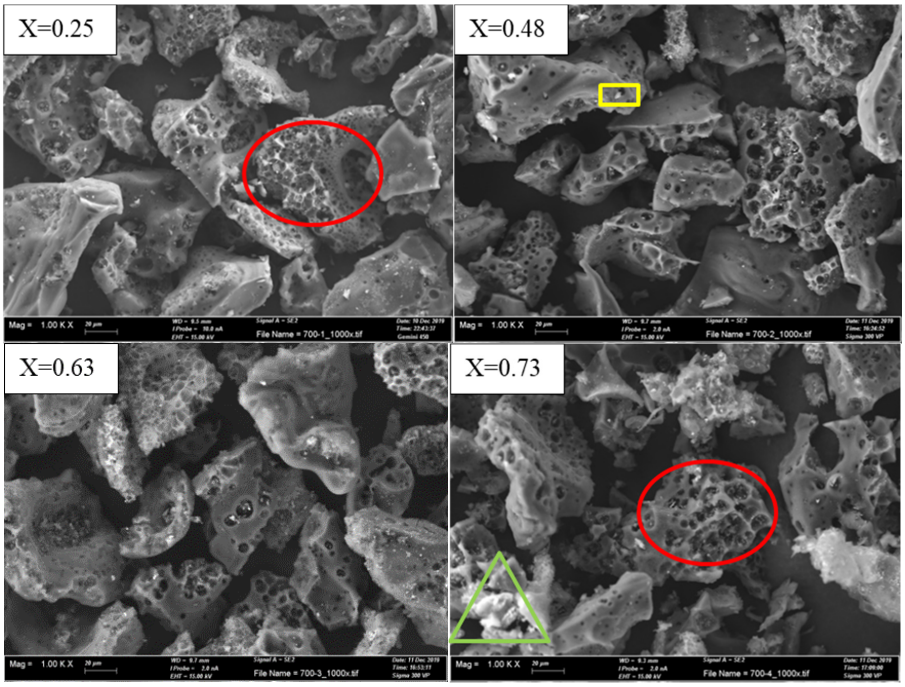

Figure 8. SEM images (1000× magnification) of char with different carbon conversions prepared from char gasification in H_2O at 700 °C.

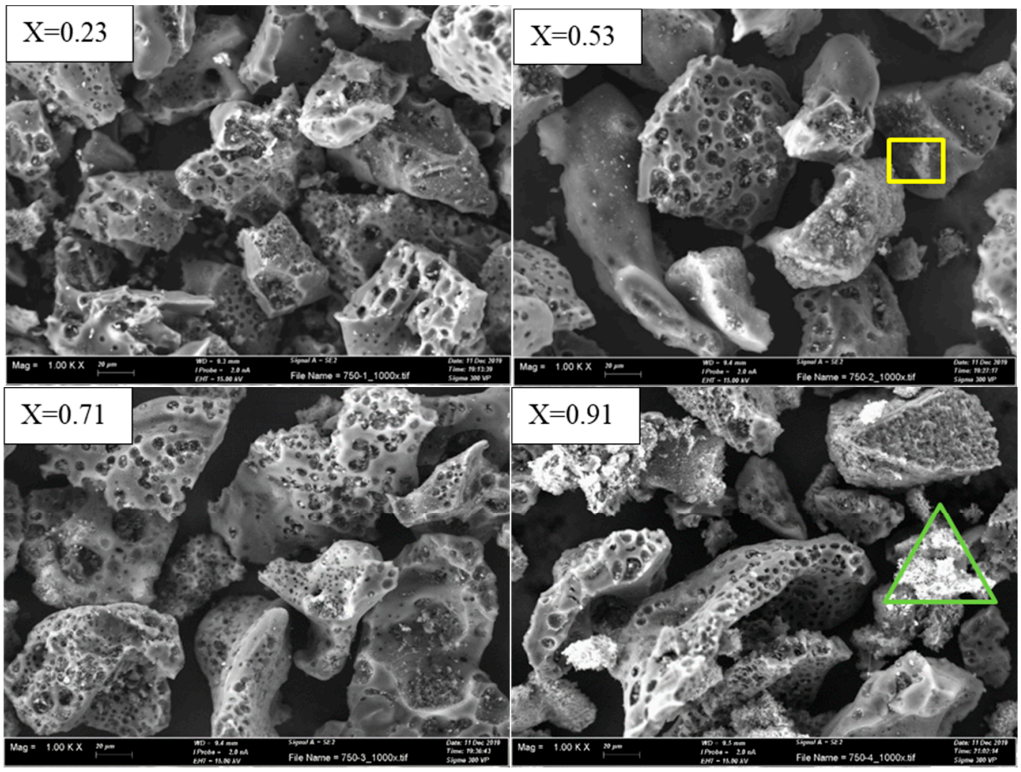

Figure 9. SEM images (1000× magnification) of char at different carbon conversions prepared from char gasification in H_2O at 750 °C.

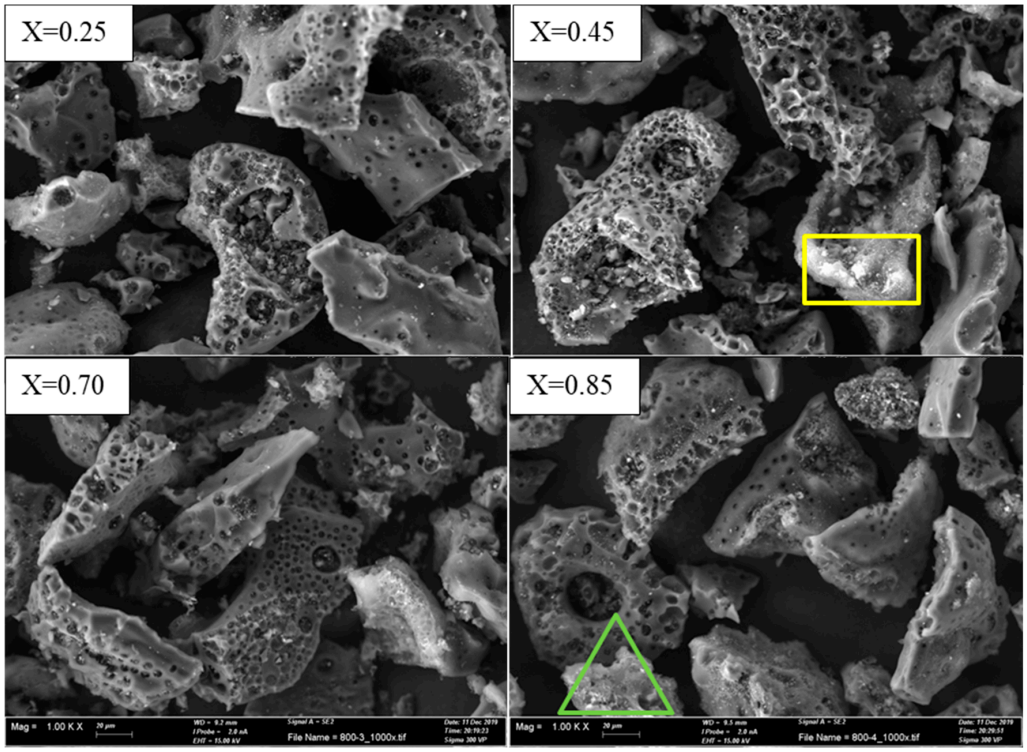

Figure 10. SEM images (1000× magnification) of char with different carbon conversions prepared from char gasification in H_2O at 800 °C.

As shown in Figure 8, honeycomb-like structures are observed on the char surface. At 25% of char conversion, the surface is more porous than the original char and more small pores are scattered on the

char surface. During the conversion of the char, the original pores are enlarged, and new pores are formed (red circle), while the char particle size is gradually decreased.

The surface of the char obtained at 750 °C, shown in Figure 9, displays macroscopic similarities to the one obtained at 700 °C with mineral particles being spread unevenly on the surface. In Figure 10, the surface morphology at 800 °C is shown and is similar to the ones at 700 and 750 °C. Mineral particles (yellow rectangle) become larger, plausibly due to an increased mobility and agglomeration at higher gasification temperatures. N.B. Klinghoffer et al. [36] observed that the agglomeration is clearly visible at 1000 °C.

The agglomerates are formed at higher conversion (green triangle) due to the increased mineral content during char consumption, which is analogous to the results obtained by Yonghui et al. [22] while investigating the morphology of chars exposed in steam atmosphere.

The surface concentration of the major AAEM species (Ca, K, Mg, and Na) at different stages of char conversion is presented in Figure 11. As the char conversion increases from 0% to ~70%, the surface concentration of Ca and Mg increases at 700 °C. However, at 750 and 800 °C, the Ca concentration decreases with temperature plausibly because of formation of larger Ca particles due to agglomeration which resulted in lower exposed Ca. The decrease should not be ascribed to volatilization, since both Ca and Mg are most likely kept as oxides in the sample, especially when the temperature is lower than 1000 °C [50]. Potassium surface concentration is positively correlated with the increase of char conversion with the exception of the low temperature gasification at 700 °C [51], which is at the lower limit of alkali salt vaporization, suggesting K to be highly mobile [50]. At all temperatures, the surface concentration of Na shows no significant change.

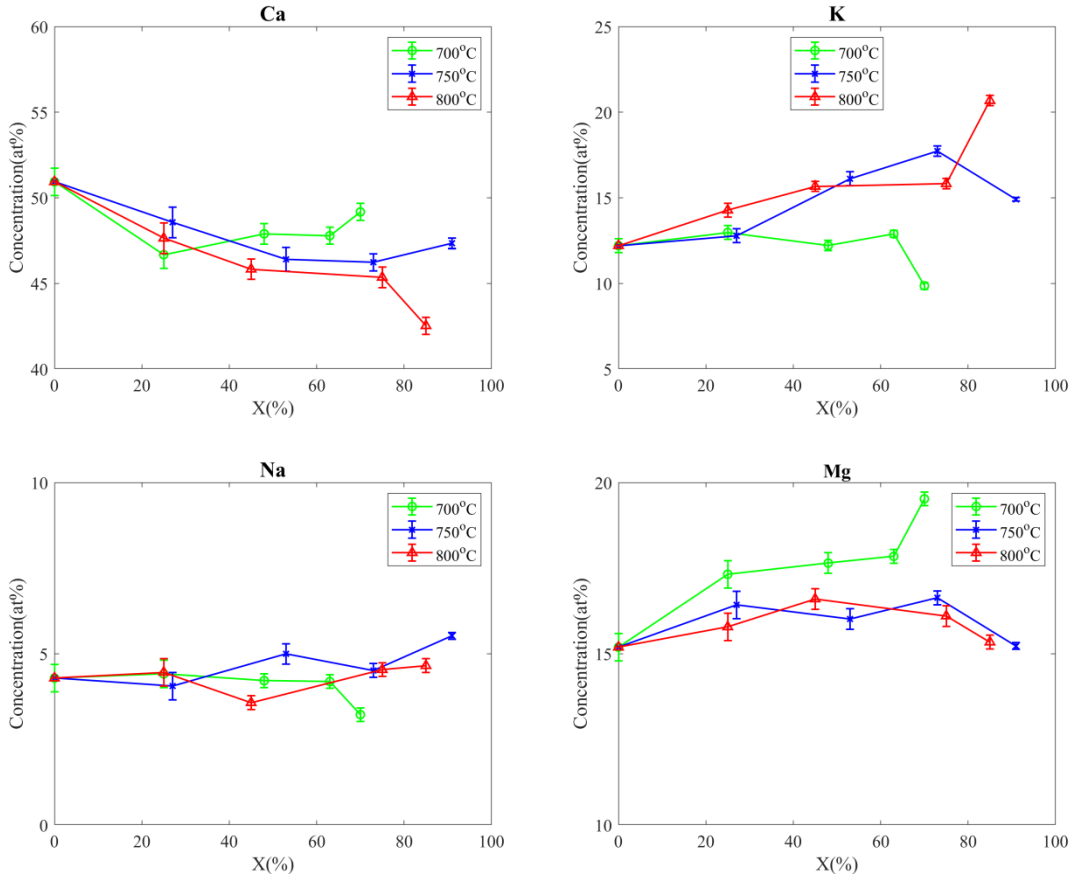

Figure 11. Surface concentrations of the alkali and alkaline earth metal (AAEM) species as a function of char conversion at different temperatures.

3.2. Water Leached Chars

In order to identify the effects of the mineral content on char conversion, gasification experiments with demineralized char were conducted. N_2-physisorption (Figure 12) of the water leached char indicate that water leaching does not affect the pore structure of the char samples. The corresponding specific surface areas are 330, 340, and 410 m^2/g for the OC, 2LC, and 48LC, respectively. The above is macroscopically verified by SEM microscopy as shown in Figures 7 and 13.

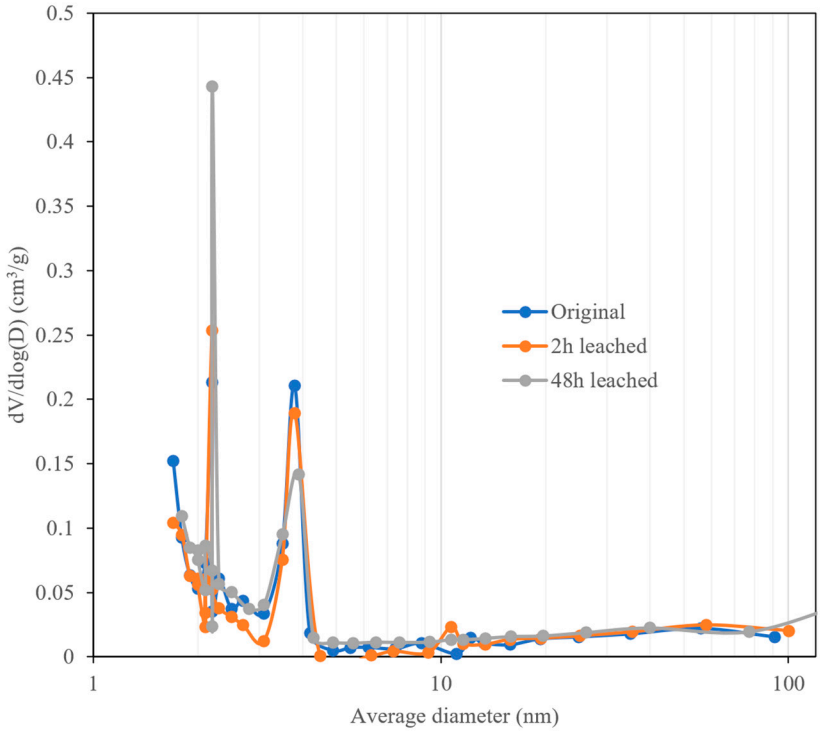

Figure 12. Pore size distribution (BJH) of original and the leached char samples.

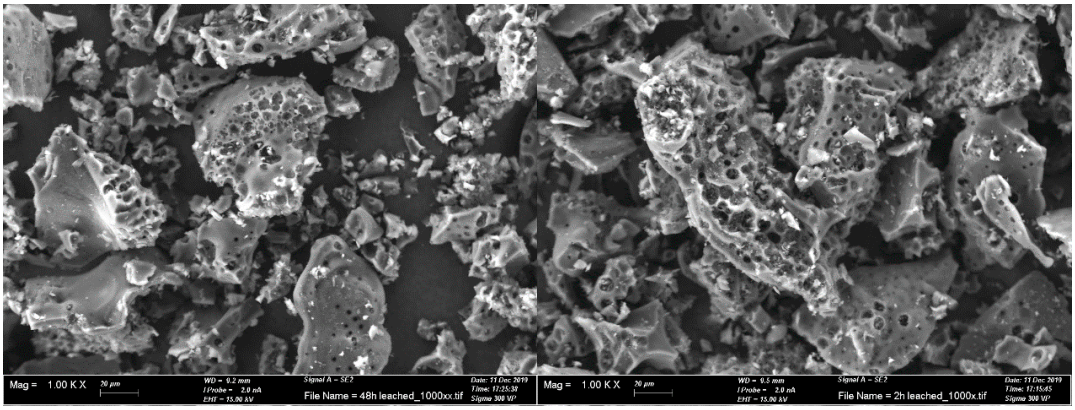

Figure 13. SEM images of 2LC and 48LC.

ICP-SFMS analysis indicated that K, Mg, and Ca are the major mineral elements in the OC, while Na, Fe, Al, and P are present in lower concentrations (Figure 14). As seen, the water leaching results in a significant reduction of the amount of K, while Ca and Mg are only slightly decreased. As similar to K, Na is also affected greatly by water leaching. Approximately 77% of Na and 86% of K were washed out after the 48 h treatment. Given that the contents of Fe, Al, and Mn are barely affected by the water treatment and the very low Na content, it is reasonable to ascribe any observed differences in reactivity to K. The importance of K in char reactivity has also been identified by Wang et al. [52].

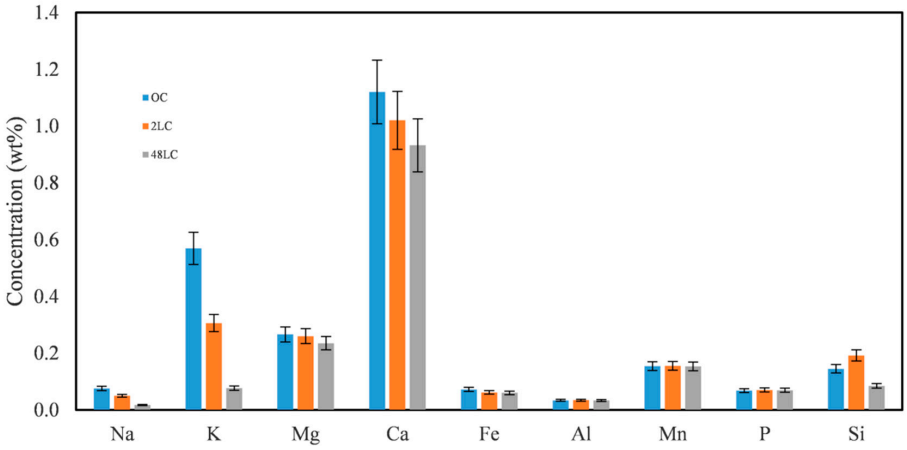

Figure 14. Effects of water leaching on the concentrations of main inorganic elements in char sample, dry basis.

The reactivities of the water-leached charrs at 700, 750, and 800 °C are shown in Figure 15. At all temperatures, OC shows a constant reactivity up to conversions of approximately 70%, where a significant increase is observed. The mildly leached sample (2LC) shows a declining reactivity up to conversion of approximately 80% where a significant increase in reactivity is observed. The reactivity of 48LC exhibits a monotonic steep decline in reactivity with conversion indicating that the increase in reactivity at the later stages of gasification is mainly attributed to the mineral content.

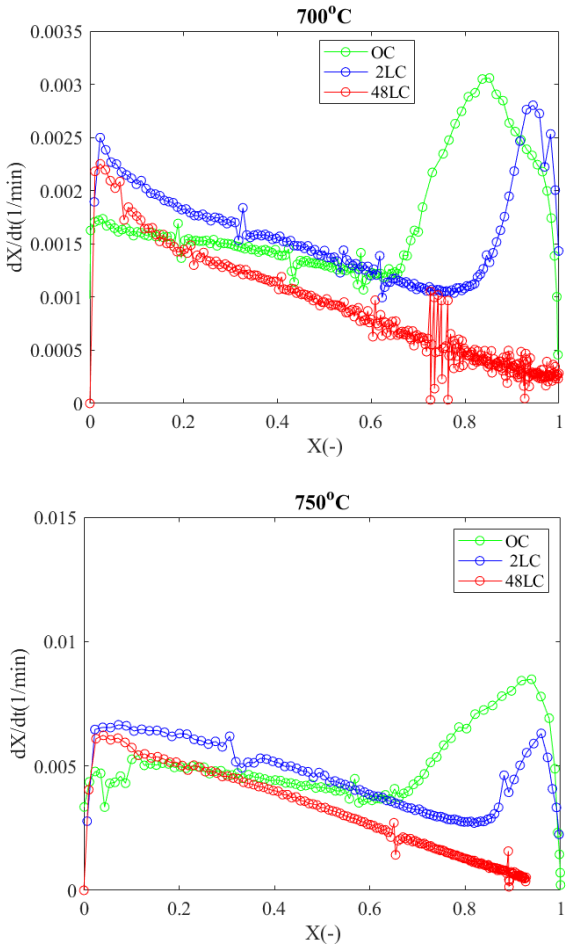

Figure 15. *Cont.*

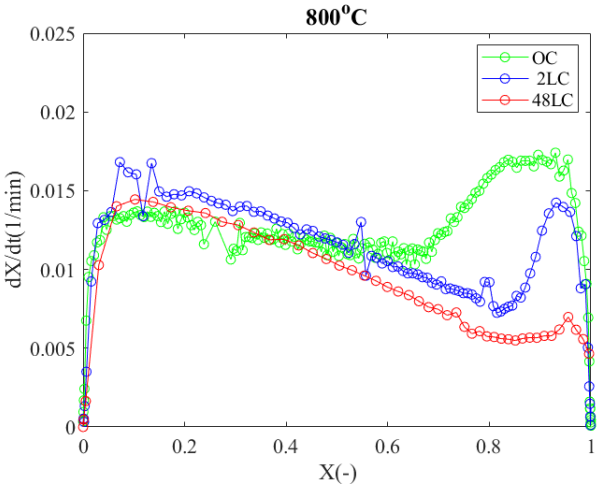

Figure 15. Gasification rate versus conversion for OC, 2LC, and 48LC at different temperatures.

4. Discussion

As shown in Figure 1, the gasifier-derived char shows a lower reactivity compared to the TGA-generated char. Albeit heating rate is known to be of importance for production of char of high reactivity both in biomass and coal gasification [9,13,53,54], the results indicate that the char generated at high heating rate (entrained flow gasifier) is not as reactive as the char generated at slow heating rate in the TGA. Another parameter which is of importance is the temperature history of the char particle. The char from entrained flow gasifier has been exposed to temperatures in excess of 1000 °C and is partly preoxidized. The degree of preoxidation and temperature are being reported to greatly affect the reactivities of coal derived chars [55,56], and therefore the observed lower reactivity can be attributed to the high preoxidation temperature the char has been subjected to in the gasifier.

It is evident (Figure 5) that during char conversion, there is a simultaneous generation of micropores and development of mesopores (and to some extent macropores at higher conversions), as a result of micropore enlargement, irrespective of the temperature. The simultaneous and uniform development are indicative of an interconnected porous network [22]. The generation of micropores suggests reaction on the active sites of char on the external surface [57] or opening of the so-called closed pores of the biochar structure [20,58] both being supported by the observed increase in char surface area and pore volume (Figure 6).

Moreover, the continuous and uniform porous network development indicates that the total particle volume is readily accessible inferring that intraparticle diffusion is not limiting the conversion, and thus the observed conversions are under kinetic control.

The reactivity behaviors observed (Figure 15) at conversions up to ~70% are a result of the total char surface area available for reaction with steam. The observed decline in the reactivity for all samples is primarily due to a decrease in the total surface area (and thus active reaction sites) in the reaction system (thermo balance), supporting that the system is under kinetic control regime [59,60]. Increased access of steam to catalytic active sites, which are gradually exposed as conversion progresses (Figures 8–10) and their surface density increase with carbon consumption, can ebhance the reactivity at later stages. Diffusion limitations have been reported to be of importance for char particle sizes in the vicinity of 300 µm at temperatures in excess of 800 °C in steam atmosphere [29,61].

The dependence on the char surface area can be elucidated by determining the specific area normalized reactivity at very low conversion with the assumption that the surface area of the initial char has not changed considerably. As listed in Table 3 the obtained normalized reactivities are comparable and the differences observed can be ascribed to the small variation in the initial surface area and porosity of the samples.

Table 3. Specific area normalized reactivity at 3% conversion.

	$(dX/dt)/S_{total}$ (g/m^2-min)		
Samples / **T (°C)**	**OC**	**2LC**	**48LC**
700	5.26×10^{-6}	7.01×10^{-6}	5.49×10^{-6}
750	1.45×10^{-5}	1.90×10^{-5}	1.49×10^{-5}
800	3.30×10^{-5}	3.81×10^{-5}	3.18×10^{-5}

As perceived, the initial surface normalized (or intrinsic) reactivity of the char is comparable irrespective of the ash content, indicating that the available char area is more important. The generation of new micropores and enlargement of existing pores (as shown in Figures 5 and 6) during conversion increases the surface area and accessibility of steam, however the consumption of carbon results in, as expected, reduced reactivity. The normalized reactivity is reduced by approximately 63%, 51%, and 25% at ~25% conversion for 700, 750, and 800 °C, respectively. Limitations due to diffusion through ash layer, similar to the shrinking core model, cannot explain the obtained results given that no extensive ash layer is formed (Figures 8–10).

The reactivity of OC albeit declining, is the least affected (for conversions up to ~70%) compared to 2LC and 48LC (Figure 15). The observed decline in reactivity is negatively correlated with the mineral content of the char, indicating that with increasing particle conversion, the contribution of the catalytic effects of the mineral content become more important. Peranders et al. [32] observed that there was a steady increase of reactivity with the increase of the alkali content (K) at char conversions up to 70%. Bouraoui et al. [29] reported that the reaction rate is strongly dependent on the K content at conversions higher than 70%, during CO_2 gasification of char, while Suzuki, T. et al. [33] observed proportional increase in gasification rates to the K content of cedar wood. The observed behavior can be related to the surface exposed minerals. As can be seen in Figure 11, the K on the char surface increases as the reaction progresses to completion. The different behavior of 48LC is therefore directly correlated to the K content.

At conversions greater than 70%, the char reactivity is increased to various degrees for all samples, indicating the aforementioned dependence on the mineral content (Figures 14 and 15). At all temperatures, the turning point of reactivity curves is observed at similar conversion (66–70%), supporting the char conversion until this point took place under kinetic controlled regime (negligible intraparticle diffusion limitations) [60]. This suggests that there are distinct regions where the superimposed phenomena of micropore structure development and alkali catalyzed reactions are prevailing.

The observed lag in the reactivity increase for 2LC and 48LC, as shown in Figure 15, can be ascribed to the reduced K content (Figure 14) and its associated catalytic activity. The onset of reactivity increase is observed at conversion of 85% and 92% for 2LC and 48LC, respectively.

For OC, the catalytic effect would lead to a continuous increase in reactivity until the conversion reaches 95% (Figure 15). For 48LC, the reaction rate decreases with conversion up to 92%. At this stage, the micropore surface area increases indicating enhanced reaction activity. Figure 16 schematically illustrates the progression of char conversion and the role of K.

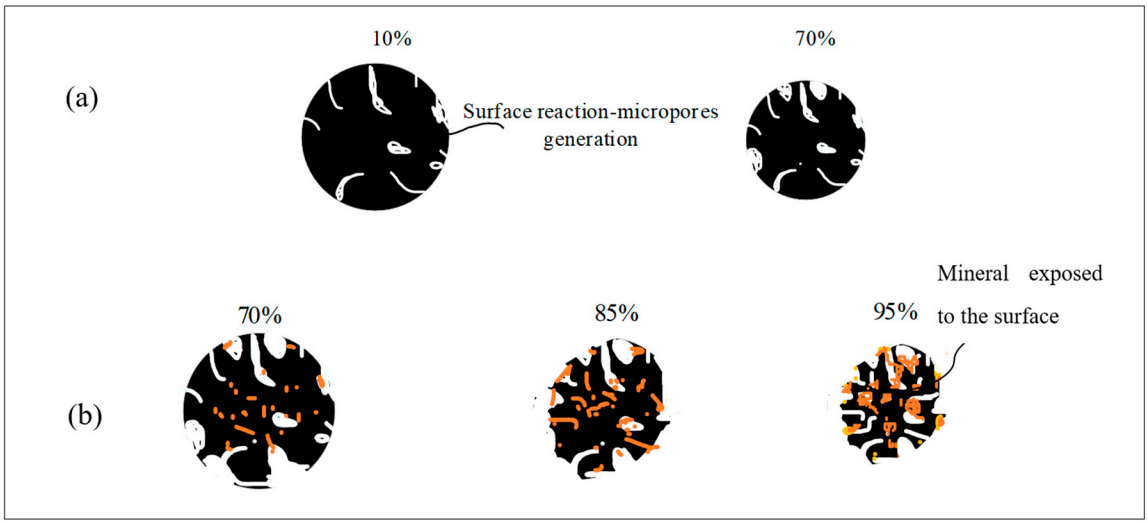

Figure 16. Simplified schematic representation of char conversion in steam atmosphere. (**a**) Progression of char conversion. (**b**) The role of K at higher char conversion.

5. Conclusions

In the present study, the evolution of char structural features and the effect of ash, during steam gasification of char residues collected from a commercial entrained flow gasifier, were investigated. Thermogravimetric analysis was used to assess the combined effects of pore structure and ash on char reactivity toward steam at a temperature range between 700 and 800 °C.

From the early conversion stages, the char particles are characterized by a broad pore size distribution that includes both micro- and mesopores at a ~1:1 volume ratio. During conversion, new micropores are generated and also existing micropores and mesopores are enlarged indicating that the whole particle volume is accessible to steam, which in turn implies that conversion takes place in the kinetic control regime. The generation of micropores and the subsequent enlargement result in substantial increase in the specific total surface area, as well as the total pore volume of char (1.3–3.1 and 2.0–5.3 times for the surface area and pore volume respectively) up to a certain conversion point, where they pivot and decrease at all temperatures. The temperature has a minor effect on char pore structure development.

At conversions below 70%, the conversion is proportional to the surface area of the char irrespective of the mineral content of the char. Declining reactivity with increasing conversion supports that conversion was taking place in kinetic regime and is proportional to char active sites.

The results indicate that the char generated at high heating rate in an entrained flow gasifier is not as reactive as the char generated at slow heating rate in the TGA. The observed lower reactivity can possibly be attributed to high preoxidation temperature that the char has been subjected in the entrained flow gasifier.

When the conversion reaches 70%, catalytic phenomena mainly due to potassium presence become dominant. From this it is evident that potassium is an important parameter to predict steam gasification reactivity for high conversion, as in the present study is determined to be above 70%, The point of conversion where the reactivity increases is clearly dependent on the K content, as illustrated by the observed differences for the original and water leached chars.

Conclusively, the study showed that the superimposed phenomena of surface area and pore development as well as catalytic reactions due to alkali presence have distinct regions where they prevail with the low conversions governed by noncatalytic reactions and micropores generation, while at high conversions the importance of catalytic reactions is greater.

Supplementary Materials: The following are available online at http://www.mdpi.com/1996-1073/13/19/5004/s1.

Author Contributions: S.D. was responsible for conceptualization, data curation, validation, formal analysis, and original draft preparation. E.K. and K.E. were responsible for the conceptualization and supervision of the project. All authors participated in the writing, review, and editing of the manuscript. All authors have read and agreed to the published version of the manuscript.

Funding: Swedish gasification Centre (SFC), Swedish Energy Agency (contract no 34721-2).

Acknowledgments: This work was carried out within the Swedish Centre for Biomass Gasification (SFC). The authors are grateful to the Swedish Energy Agency for financial support. The authors appreciate the industrial partner (Meva Energy) for supplying the sample.

Conflicts of Interest: The authors declare no conflict of interest.

References

1. Acharya, B.; Dutta, A.; Basu, P. An investigation into steam gasification of biomass for hydrogen enriched gas production in presence of CaO. *Int. J. Hydrogen Energy* **2010**, *35*, 1582–1589. [CrossRef]
2. Rauch, R.; Hrbek, J.; Hofbauer, H. Biomass gasification for synthesis gas production and applications of the syngas. *WIREs Energy Environ.* **2014**, *3*, 343–362. [CrossRef]
3. Ahmed, I.I.; Gupta, A.K. Kinetics of woodchips char gasification with steam and carbon dioxide. *Appl. Energy* **2011**, *88*, 1613–1619. [CrossRef]
4. Laurendeau, N.M. Heterogeneous kinetics of coal char gasification and combustion. *Prog. Energy Combust. Sci.* **1978**, *4*, 221–270. [CrossRef]
5. Smith, I.W. The combustion rates of coal chars: A review. *Symp. (Int.) Combust.* **1982**, *19*, 1045–1065. [CrossRef]
6. Bews, I.M.; Hayhurst, A.N.; Richardson, S.M.; Taylor, S.G. The order, Arrhenius parameters, and mechanism of the reaction between gaseous oxygen and solid carbon. *Combust. Flame* **2001**, *124*, 231–245. [CrossRef]
7. Hurt, R.H.; Calo, J.M. Semi-global intrinsic kinetics for char combustion modeling. *Combust. Flame* **2001**, *125*, 1138–1149. [CrossRef]
8. Encinar, J.M.; González, J.F.; Rodríguez, J.J.; Ramiro, M.J. Catalysed and uncatalysed steam gasification of eucalyptus char: Influence of variables and kinetic study. *Fuel* **2001**, *80*, 2025–2036. [CrossRef]
9. Di Blasi, C. Combustion and gasification rates of lignocellulosic chars. *Prog. Energy Combust. Sci.* **2009**, *35*, 121–140. [CrossRef]
10. Guizani, C.; Jeguirim, M.; Valin, S.; Limousy, L.; Salvador, S. Biomass Chars: The Effects of Pyrolysis Conditions on their Morphology, Structure, Chemical Properties and Reactivity. *Energies* **2017**, *10*, 796. [CrossRef]
11. Septien, S.; Escudero Sanz, F.J.; Salvador, S.; Valin, S. The effect of pyrolysis heating rate on the steam gasification reactivity of char from woodchips. *Energy* **2018**, *142*, 68–78. [CrossRef]
12. Avila, C.; Pang, C.H.; Wu, T.; Lester, E. Morphology and reactivity characteristics of char biomass particles. *Bioresour. Technol.* **2011**, *102*, 5237–5243. [CrossRef]
13. Mermoud, F.; Salvador, S.; Van de Steene, L.; Golfier, F. Influence of the pyrolysis heating rate on the steam gasification rate of large wood char particles. *Fuel* **2006**, *85*, 1473–1482. [CrossRef]
14. Senneca, O. Kinetics of pyrolysis, combustion and gasification of three biomass fuels. *Fuel Process. Technol.* **2007**, *88*, 87–97. [CrossRef]
15. Gil, M.V.; Riaza, J.; Álvarez, L.; Pevida, C.; Rubiera, F. Biomass devolatilization at high temperature under N_2 and CO_2: Char morphology and reactivity. *Energy* **2015**, *91*, 655–662. [CrossRef]
16. Bai, Y.; Wang, Y.; Zhu, S.; Li, F.; Xie, K. Structural features and gasification reactivity of coal chars formed in Ar and CO_2 atmospheres at elevated pressures. *Energy* **2014**, *74*, 464–470. [CrossRef]
17. Guizani, C.; Jeguirim, M.; Gadiou, R.; Escudero Sanz, F.J.; Salvador, S. Biomass char gasification by H_2O, CO_2 and their mixture: Evolution of chemical, textural and structural properties of the chars. *Energy* **2016**, *112*, 133–145. [CrossRef]
18. Fu, P.; Hu, S.; Xiang, J.; Yi, W.; Bai, X.; Sun, L.; Su, S. Evolution of char structure during steam gasification of the chars produced from rapid pyrolysis of rice husk. *Bioresour. Technol.* **2012**, *114*, 691–697. [CrossRef]
19. Keown, D.M.; Hayashi, J.-I.; Li, C.-Z. Drastic changes in biomass char structure and reactivity upon contact with steam. *Fuel* **2008**, *87*, 1127–1132. [CrossRef]

20. Wu, H.; Yip, K.; Tian, F.; Xie, Z.; Li, C.-Z. Evolution of Char Structure during the Steam Gasification of Biochars Produced from the Pyrolysis of Various Mallee Biomass Components. *Ind. Eng. Chem. Res.* **2009**, *48*, 10431–10438. [CrossRef]
21. Kajita, M.; Kimura, T.; Norinaga, K.; Li, C.-Z.; Hayashi, J.-I. Catalytic and Noncatalytic Mechanisms in Steam Gasification of Char from the Pyrolysis of Biomass. *Energy Fuels* **2010**, *24*, 108–116. [CrossRef]
22. Bai, Y.; Lv, P.; Yang, X.; Gao, M.; Zhu, S.; Yan, L.; Li, F. Gasification of coal char in H_2O/CO_2 atmospheres: Evolution of surface morphology and pore structure. *Fuel* **2018**, *218*, 236–246. [CrossRef]
23. Alvarez, J.; Lopez, G.; Amutio, M.; Bilbao, J.; Olazar, M. Evolution of biomass char features and their role in the reactivity during steam gasification in a conical spouted bed reactor. *Energy Convers. Manag.* **2019**, *181*, 214–222. [CrossRef]
24. Davidsson, K.O.; Korsgren, J.G.; Pettersson, J.B.C.; Jäglid, U. The effects of fuel washing techniques on alkali release from biomass. *Fuel* **2002**, *81*, 137–142. [CrossRef]
25. Di Blasi, C.; Branca, C.; D'Errico, G. Degradation characteristics of straw and washed straw. *Thermochim. Acta* **2000**, *364*, 133–142. [CrossRef]
26. Jenkins, B.M.; Bakker, R.R.; Wei, J.B. On the properties of washed straw. *Biomass Bioenergy* **1996**, *10*, 177–200. [CrossRef]
27. Zolin, A.; Jensen, A.; Jensen, P.A.; Frandsen, F.; Dam-Johansen, K. The Influence of Inorganic Materials on the Thermal Deactivation of Fuel Chars. *Energy Fuels* **2001**, *15*, 1110–1122. [CrossRef]
28. Aho, A.; DeMartini, N.; Pranovich, A.; Krogell, J.; Kumar, N.; Eränen, K.; Holmbom, B.; Salmi, T.; Hupa, M.; Murzin, D.Y. Pyrolysis of pine and gasification of pine chars-influence of organically bound metals. *Bioresour. Technol.* **2013**, *128*, 22–29. [CrossRef]
29. Bouraoui, Z.; Dupont, C.; Jeguirim, M.; Limousy, L.; Gadiou, R. CO_2 gasification of woody biomass chars: The influence of K and Si on char reactivity. *C. R. Chim.* **2016**, *19*, 457–465. [CrossRef]
30. Huang, Y.; Yin, X.; Wu, C.; Wang, C.; Xie, J.; Zhou, Z.; Ma, L.; Li, H. Effects of metal catalysts on CO_2 gasification reactivity of biomass char. *Biotechnol. Adv.* **2009**, *27*, 568–572. [CrossRef]
31. Karlström, O.; Dirbeba, M.J.; Costa, M.; Brink, A.; Hupa, M. Influence of K/C Ratio on Gasification Rate of Biomass Chars. *Energy Fuels* **2018**, *32*, 10695–10700. [CrossRef]
32. Perander, M.; DeMartini, N.; Brink, A.; Kramb, J.; Karlström, O.; Hemming, J.; Moilanen, A.; Konttinen, J.; Hupa, M. Catalytic effect of Ca and K on CO_2 gasification of spruce wood char. *Fuel* **2015**, *150*, 464–472. [CrossRef]
33. Suzuki, T.; Nakajima, H.; Ikenaga, N.-O.; Oda, H.; Miyake, T. Effect of mineral matters in biomass on the gasification rate of their chars. *Biomass Conv. Bioref.* **2011**, *1*, 17–28. [CrossRef]
34. Kirtania, K.; Axelsson, J.; Matsakas, L.; Christakopoulos, P.; Umeki, K.; Furusjö, E. Kinetic study of catalytic gasification of wood char impregnated with different alkali salts. *Energy* **2017**, *118*, 1055–1065. [CrossRef]
35. Kelebopile, L.; Sun, R.; Liao, J. Fly ash and coal char reactivity from Thermo-gravimetric (TGA) experiments. *Fuel Process. Technol.* **2011**, *92*, 1178–1186. [CrossRef]
36. Klinghoffer, N.B.; Castaldi, M.J.; Nzihou, A. Influence of char composition and inorganics on catalytic activity of char from biomass gasification. *Fuel* **2015**, *157*, 37–47. [CrossRef]
37. Jing, X.; Wang, Z.; Yu, Z.; Zhang, Q.; Li, C.; Fang, Y. Experimental and Kinetic Investigations of CO_2 Gasification of Fine Chars Separated from a Pilot-Scale Fluidized-Bed Gasifier. *Energy Fuels* **2013**, *27*, 2422–2430. [CrossRef]
38. Gu, J.; Wu, S.; Wu, Y.; Li, Y.; Gao, J. Differences in Gasification Behaviors and Related Properties between Entrained Gasifier Fly Ash and Coal Char. *Energy Fuels* **2008**, *22*, 4029–4033. [CrossRef]
39. Zhang, H.; Zhu, Z.; Dong, Q.; Yu, K.; Lu, Q. Structural Properties and Gasification Reactivity of Shenmu Fly Ash Obtained from a 5t/d Circulating Fluidized Bed Gasifier. *Procedia Eng.* **2015**, *102*, 1104–1111. [CrossRef]
40. Zhang, Y.; Zhang, H.; Zhu, Z. Regasification properties of industrial CFB-gasified semi-char. *J. Therm. Anal. Calorim.* **2018**, *131*, 3035–3046. [CrossRef]
41. Meng, X.; Benito, P.; de Jong, W.; Basile, F.; Verkooijen, A.H.M.; Fornasari, G.; Vaccari, A. Steam–O_2 Blown Circulating Fluidized-Bed (CFB) Biomass Gasification: Characterization of Different Residual Chars and Comparison of Their Gasification Behavior to Thermogravimetric (TG)-Derived Pyrolysis Chars. *Energy Fuels* **2012**, *26*, 722–739. [CrossRef]
42. Marquez-Montesinos, F.; Cordero, T.; Rodrıguez-Mirasol, J.; Rodrıguez, J.J. CO_2 and steam gasification of a grapefruit skin char. *Fuel* **2002**, *81*, 423–429. [CrossRef]

43. Dupont, C.; Jacob, S.; Marrakchy, K.O.; Hognon, C.; Grateau, M.; Labalette, F.; Da Silva Perez, D. How inorganic elements of biomass influence char steam gasification kinetics. *Energy* **2016**, *109*, 430–435. [CrossRef]
44. Dupont, C.; Nocquet, T.; Da Costa, J.A.; Verne-Tournon, C. Kinetic modelling of steam gasification of various woody biomass chars: Influence of inorganic elements. *Bioresour. Technol.* **2011**, *102*, 9743–9748. [CrossRef] [PubMed]
45. Hognon, C.; Dupont, C.; Grateau, M.; Delrue, F. Comparison of steam gasification reactivity of algal and lignocellulosic biomass: Influence of inorganic elements. *Bioresour. Technol.* **2014**, *164*, 347–353. [CrossRef] [PubMed]
46. Yip, K.; Tian, F.; Hayashi, J.-I.; Wu, H. Effect of Alkali and Alkaline Earth Metallic Species on Biochar Reactivity and Syngas Compositions during Steam Gasification. *Energy Fuels* **2010**, *24*, 173–181. [CrossRef]
47. Ohki, A.; Nakajima, T.; Yamashita, H.; Iwashita, A.; Takanashi, H. Leaching of various metals from coal into aqueous solutions containing an acid or a chelating agent. *Fuel Process. Technol.* **2004**, *85*, 1089–1102. [CrossRef]
48. Haul, R. S. J. Gregg, K. S. W. Sing: Adsorption, Surface Area and Porosity. 2. Auflage, Academic Press, London 1982. 303 Seiten, Preis: 49.50. *Berichte der Bunsengesellschaft für Physikalische Chemie* **1982**, *86*, 957. [CrossRef]
49. Ioannidou, O.; Zabaniotou, A. Agricultural residues as precursors for activated carbon production—A review. *Renew. Sustain. Energy Rev.* **2007**, *11*, 1966–2005. [CrossRef]
50. Defoort, F.; Dupont, C.; Durruty, J.; Guillaudeau, J.; Bedel, L.; Ravel, S.; Campargue, M.; Labalette, F.; Da Silva Perez, D. Thermodynamic Study of the Alkali Release Behavior during Steam Gasification of Several Biomasses. *Energy Fuels* **2015**, *29*, 7242–7253. [CrossRef]
51. Moud, P.H.; Andersson, K.J.; Lanza, R.; Pettersson, J.B.C.; Engvall, K. Effect of gas phase alkali species on tar reforming catalyst performance: Initial characterization and method development. *Fuel* **2015**, *154*, 95–106. [CrossRef]
52. Wang, M.; Shen, Y.; Guo, P.; Kong, J.; Wu, Y.; Chang, L.; Wang, J.; Xie, W. A comparative study on the intrinsic reactivity and structural evolution during gasification of chars from biomass and different rank coals. *J. Anal. Appl. Pyrolysis* **2020**, *149*, 104859. [CrossRef]
53. Ashu, J.T.; Nsakala, N.Y.; Mahajan, O.P.; Walker, P.L. Enhancement of char reactivity by rapid heating of precursor coal. *Fuel* **1978**, *57*, 250–251. [CrossRef]
54. Cetin, E.; Moghtaderi, B.; Gupta, R.; Wall, T.F. Influence of pyrolysis conditions on the structure and gasification reactivity of biomass chars. *Fuel* **2004**, *83*, 2139–2150. [CrossRef]
55. Gomi, K.; Hishinuma, Y. Effect of pre-oxidation on reactivity of chars in steam. *Fuel* **1982**, *61*, 77–80. [CrossRef]
56. Tremel, A.; Haselsteiner, T.; Nakonz, M.; Spliethoff, H. Coal and char properties in high temperature entrained flow gasification. *Energy* **2012**, *45*, 176–182. [CrossRef]
57. Fatehi, H.; Bai, X.-S. Structural evolution of biomass char and its effect on the gasification rate. *Appl. Energy* **2017**, *185*, 998–1006. [CrossRef]
58. Struis, R.P.W.J.; Von Scala, C.; Stucki, S.; Prins, R. Gasification reactivity of charcoal with CO_2. Part I: Conversion and structural phenomena. *Chem. Eng. Sci.* **2002**, *57*, 3581–3592. [CrossRef]
59. Hodge, E.M.; Roberts, D.G.; Harris, D.J.; Stubington, J.F. The Significance of Char Morphology to the Analysis of High-Temperature Char–CO_2 Reaction Rates. *Energy Fuels* **2010**, *24*, 100–107. [CrossRef]
60. Naredi, P.; Pisupati, S.V. Interpretation of Char Reactivity Profiles Obtained Using a Thermogravimetric Analyzer. *Energy Fuels* **2008**, *22*, 317–320. [CrossRef]
61. Guizani, C.; Escudero Sanz, F.J.; Salvador, S. Influence of temperature and particle size on the single and mixed atmosphere gasification of biomass char with H_2O and CO_2. *Fuel Process. Technol.* **2015**, *134*, 175–188. [CrossRef]